

Effect of particle size distribution on the effective dielectric permittivity of saturated granular media

D. A. Robinson and S. P. Friedman

The Institute of Soil, Water and Environmental Sciences, The Volcani Center, Bet Dagan, Israel

Abstract. The effective permittivity of an unconsolidated porous material is shown to be not only a function of the permittivity of the individual components but also of the distribution of particle sizes present. Increasing width of particle size distribution for glass spheres and sieved quartz sand is demonstrated to reduce the effective permittivity of a mixture compared to the effective permittivity of the corresponding monosize material. The results are shown to lie between predictions made using the *Maxwell-Garnett* [1904] formula for monosize spheres and a self-similar model [Sen *et al.*, 1981] and can be predicted by a multiple Maxwell-Garnett-based mixing model. The results demonstrate that the degree of sorting of a material will directly influence the effective permittivity of the mixture. This is beyond the effect of the change in permittivity caused by the significant change in porosity resulting from the mixing of different particle sizes.

1. Introduction

Measurements of effective permittivity have become popular for estimating the volumetric water content of porous media. The water content of soil is often estimated using the empirical formulae of Topp *et al.* [1980]. Kraszewski and Nelson [1996] have presented extensive work estimating the water content of grains from measurements of effective permittivity, while in petroleum engineering, permittivity measurements have been used to estimate the porosity of oil reservoir rock formations [Poley *et al.*, 1978]. Improved physical understanding of the system should improve estimates of water content from measurements of effective permittivity. Jones and Friedman [2000] have demonstrated that particle shape in the form of platy particles can reduce the permittivity of an unconsolidated media, the magnitude of which was found to depend on the orientation of the mica particles with the applied electrical field. The focus of this paper is not on the shape of the particles but on the effect of particle size distribution on the effective permittivity (ϵ_{eff}) measured in granular materials. The subject is introduced by briefly referring to findings from similar studies on electrical and hydraulic conductivity.

Electrical conductivity is widely used to characterize rock formations for which Archie's [1942] law, $EC_a/EC_w = 1/F = a\phi^m$, provides an important part of electric-log interpretation. EC_a is the apparent electrical conductivity of the bulk material (S m^{-1}), and EC_w is the electrical conductivity of the solution (S m^{-1}), F is the formation factor, ϕ is the porosity, a is an empirical parameter usually set to unity, and m is an empirical parameter, termed the cementation index. A modeling study by Chiew and Glandt [1987] suggested that the apparent electrical conductivity of a polydisperse system would be sensitive to the particle size distribution. Guyon *et al.* [1987] and Lemaitre *et al.* [1988] conducted experimental studies on the formation factor of binary mixtures of glass spheres; Guyon *et al.* used fused mixtures of beads. In the more detailed latter study on unconsolidated media, Lemaitre *et al.* found that there was

a small but noticeable increase in the formation factor as the diameter ratio between the two particle sizes increased. Tyc *et al.* [1988] also demonstrated that the use of a geometric model accounting for a bimodal distribution of particle sizes (sand and clay) improved the prediction of the permittivity and conductivity with measurements on rocks.

Masch and Denny [1966] presented similar findings for hydraulic conductivity. In an experimental study they demonstrated reduced permeability for unconsolidated sands with a bimodal particle size distribution as compared with a unimodal distribution.

Knowing that a particle size distribution effect had been measured for both the electrical conductivity and permeability, the challenge in this work was to see if we could measure the expected, small effect of a bimodal particle size distribution on the effective permittivity of a granular material. The concern of this paper is not that of sand-clay mixtures [Knoll and Knight, 1994] but of mixtures of particles with similar orders of magnitude. The present study only examines the high-frequency effective permittivity of relatively lossless materials. Therefore the effective permittivity (ϵ_{eff}) can be considered to be the real part of the relative permittivity (ϵ'/ϵ_0). The use of a time domain reflectometer (TDR) for making the dielectric measurements ensures that they are conducted at long wavelengths, which means that there is no scattering due to the size of the grains. Grain size can also affect the dispersion characteristics when charged surfaces are present [Chew and Sen, 1982]; however, the materials used in this study were free of surface charges. Experimental work and modeling based on the *Maxwell-Garnett* [1904] dielectric mixing formula are used to demonstrate the effect of the particle size distribution on the effective permittivity.

2. Theory and Modeling

Many formulae have been proposed describing the permittivity of a composite dielectric [Sihvola, 1996]. In this work we focus on a two-phase mixture of solid and water. The theoretical approach follows that of the *Lord Rayleigh* [1892] mixing formula,

Copyright 2001 by the American Geophysical Union.

Paper number 2000WR900227.
0043-1397/01/2000WR900227\$09.00

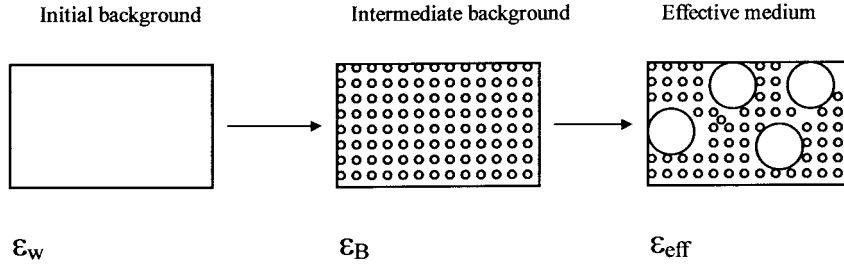


Figure 1. Schematic diagram representing the two mixing stages; ε_1 mixed into ε_0 to form the background ε_B and then ε_2 mixed into ε_B to give the effective permittivity ε_{eff} .

$$\frac{\varepsilon_{\text{eff}} - \varepsilon_0}{\varepsilon_{\text{eff}} + 2\varepsilon_0} = f \frac{\varepsilon_1 - \varepsilon_0}{\varepsilon_1 + 2\varepsilon_0}, \quad (1)$$

where a small volumetric fraction of $f = (1 - \phi)$ of spherical inclusions with a permittivity of ε_1 are embedded as isolated spheres in a background or host dielectric ε_0 and ε_{eff} is the effective permittivity of the mixture. Written explicitly for the effective permittivity of a two-component mixture, it is known as the *Maxwell-Garnett* [1904] formula:

$$\varepsilon_{\text{eff}} = \varepsilon_0 + 3f\varepsilon_0 \left[\frac{\varepsilon_1 - \varepsilon_0}{\varepsilon_1 + 2\varepsilon_0 - f(\varepsilon_1 - \varepsilon_0)} \right]. \quad (2)$$

Its explicit form and the fact that it satisfies the limiting cases for either a vanishing inclusion phase or host phase has led to its application in many fields [Sihvola, 1997].

Equation (1) formed the basis of a self-similar model presented by *Sen et al.* [1981]. These investigators set out to develop a model, which would describe the permittivity of saturated porous rocks. The sequential additions of the inclusion solid phase into the host water phase allowed them to mix the solid dielectric into a background of water so that the conceptual pore network would remain intact to low values of porosity such as encountered in rocks. The derivation is given by *Sen et al.* [1981] and results in

$$\left(\frac{\varepsilon_1 - \varepsilon_{\text{eff}}}{\varepsilon_1 - \varepsilon_0} \right) \left(\frac{\varepsilon_0}{\varepsilon_{\text{eff}}} \right)^{1/3} = \phi. \quad (3)$$

The model presented by *Sen et al.* [1981] should apply to a fractal medium of infinitely wide particle size distribution (PSD) and should therefore form a lower bound for the estimate of the permittivity of a real porous system made of spherical grains of bounded PSD. These two equations (2) and (3) should therefore form the upper and lower bounds for real granular materials.

The present modeling approach is presented diagrammatically in Figure 1 and starts with the smallest size fraction (ε_{1a}), with permittivity of 5 and volumetric fraction (f_1) being mixed into the background of water (ε_0) of volumetric fraction (ϕ) to obtain an effective permittivity (ε_B) for this intermediate mixture:

$$\varepsilon_B = \varepsilon_0 + 3 \left(\frac{f_1}{\phi + f_1} \right) \varepsilon_0 \left[\frac{\varepsilon_{1a} - \varepsilon_0}{\varepsilon_{1a} + 2\varepsilon_0 - \left(\frac{f_1}{\phi + f_1} \right) (\varepsilon_{1a} - \varepsilon_0)} \right]. \quad (4a)$$

We then treat ε_B as the background and mix the next solid size fraction (ε_{1b}) of volumetric fraction f_2 into the intermediate ε_B background to get

$$\varepsilon_{\text{eff}} = \varepsilon_B + 3f_2\varepsilon_B \left[\frac{\varepsilon_{1b} - \varepsilon_B}{\varepsilon_{1b} + 2\varepsilon_B - f_2(\varepsilon_{1b} - \varepsilon_B)} \right]. \quad (4b)$$

As a result, an incremental mixing is developed based on the number of size fractions present, n , to give the value of the final effective permittivity of the mixture, the general equation being

$$\varepsilon_{\text{eff}} = \varepsilon_{B(n-1)} + 3f_n\varepsilon_{B(n-1)} \left[\frac{\varepsilon_1 - \varepsilon_{B(n-1)}}{\varepsilon_1 + 2\varepsilon_{B(n-1)} - f_n(\varepsilon_1 - \varepsilon_{B(n-1)})} \right]. \quad (4c)$$

Figures 2a and 2b demonstrate this mixing approach for a binary system of small and large spheres. Figure 2a is for a two-phase mixture of solid ($\varepsilon_s = 5$) in water ($\varepsilon_w = 80$) for a range of porosities from 0.2 to 0.5. Figure 2b is for solid ($\varepsilon_s = 5$) mixed in air ($\varepsilon_a = 1$). This method of mixing particle sizes, compared to monosize, results in a reduced permittivity when the background has a higher permittivity than the inclusions and in an increased permittivity when the background has a lower permittivity. The computed permittivity differences are small on a relative basis. However, for the water-saturated case some effect should be measurable, though this is working close to the accuracy limits of permittivity measurement using TDR and presents some experimental challenge.

As an intermediate conceptual stage between binary and multiple size fractions, we refer to a tertiary system of small, medium, and large particles surrounding each other. Conceptually, this should not be associated with the common soil textural division of sand, silt, and clay but can be thought of more as fine, medium, and course sand. The computed effective permittivities of the different combinations of the three volumetric fractions for a porosity of 40% completely saturated with water are presented in Figure 3. Note here that the minimum permittivity is not simply at the geometric center, i.e., one third of each of the small, medium, and large particles. It occurs at the point where the medium size fraction forms one third of the mixture (0.33) and the small and large fraction forms two thirds (0.67) but in the ratio of about one third small to two thirds large, thus forming fractions of the solid of small (0.25), medium (0.33), and large (0.42).

Figure 4 demonstrates the reduction in the permittivity expected according to the scheme presented in (4a), (4b), and (4c) for mixtures with n equal volumetric fractions of increasing particle size. The change in permittivity is consistent for porosities ranging between 0.2 and 0.5 which are representative of real systems. The initial decrease in effective permittivity is the largest for the first two mixes accounting for effective

permittivity drops of ~ 1 and ~ 0.5 , respectively. At infinite numbers of mixing steps the permittivity is reduced by ~ 3 compared with the value for monosize spheres. One can see how for very large numbers of mixes this approach converges to the *Sen et al.* [1981] model as expected.

3. Materials and Methods

Three sets of experiments were conducted, two involving glass beads and one with quartz sand. A description of the materials is followed by a more detailed description of the measurement techniques and experimental procedure, which was the same for the different packings of materials.

3.1. Granular Materials

Experiments were conducted using two sets of granular media, well-characterized glass beads and quartz sand; their physical properties are displayed in Table 1. Highly spherical soda-lime silicate glass beads (Mo-Sci Corp., Rolla, Missouri, United States of America) were used. No permittivity information was available; however, *von Hippel* [1954, p. 309] reports a relative permittivity of 6.75 at 100 MHz for soda-lime silicate glass. The quartz sand was collected from the Yerucham Crator, Negev desert, Israel, and prepared in the laboratory by acid washing and sieving. A value of $s = 4.3$ was

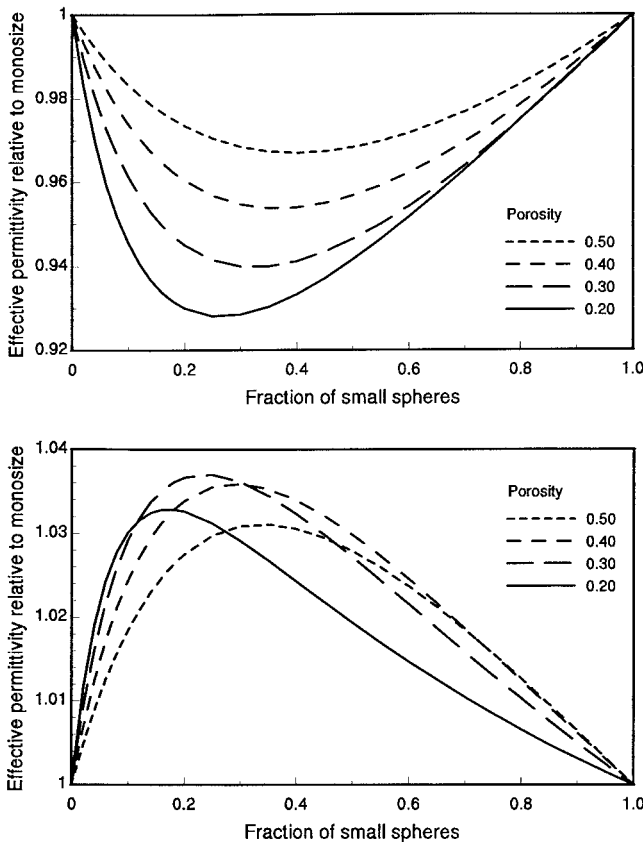


Figure 2. (a) The reduction of the effective permittivity of a binary mixture of spheres in water, relative to monosize, for a selection of porosities, calculated using the Maxwell-Garnett-based mixing model. (b) The minor increase of the effective permittivity of a binary mixture of spheres in air, relative to monosize, for a selection of porosities, calculated using the Maxwell-Garnett-based mixing model.

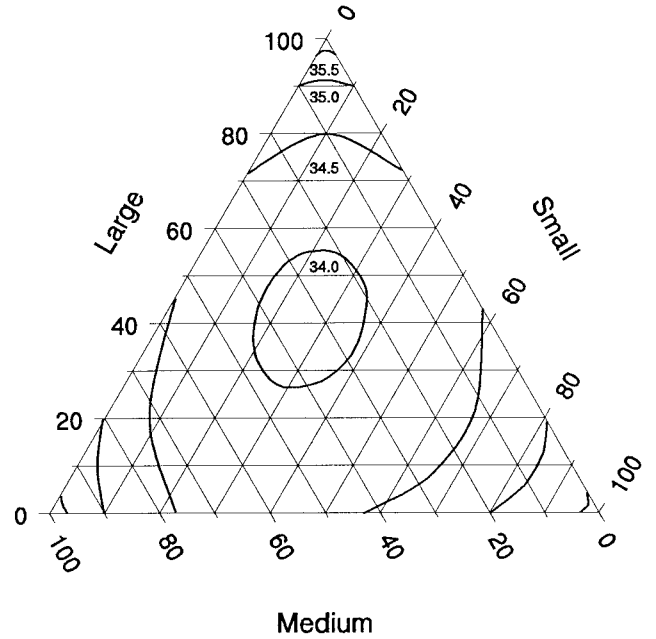


Figure 3. A triangular contour plot showing the distribution of effective permittivity for three-step mixing of small, medium, and large grains with a porosity of 0.4, ϵ_s of 5, and ϵ_w of 80.

assumed for the permittivity of the quartz based on results presented by *Carmichael* [1982] and *Lange* [1966]; this value was used in all the subsequent modeling.

3.2. Measurement of Effective Permittivity

A Tektronix (1502C) TDR cable tester was used throughout the experiments to measure the effective permittivity. The time domain reflectometer (TDR) was connected to a PC, which was used to collect and analyze the waveforms using software developed by *Heimovaara* [1993]. The TDR was connected via a 2 m, 50 ohm RG 58 coaxial cable to a purpose-built sample container. The sample container was a rectangular box constructed from Plexiglas with internal dimensions of 0.18 m long, 0.07 m wide, and 0.1 m high. The waveguide, consisting of

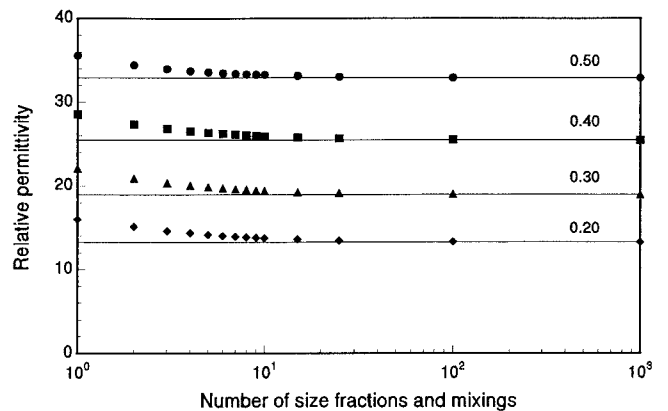


Figure 4. The effective permittivity of mixtures of selected porosity according to the number of size fractions mixed, use of equations (4a), (4b), and (4c). Note as the number of mixing steps increases, the values of permittivity converge to those predicted using the *Sen et al.* [1981] equation (3), represented by the solid lines.

Table 1. Properties of Granular Materials

Medium, μm	Size Fractions, μm	Particle Density, g cm^{-3}	ϵ_s Used in Calculations
Glass beads			
500	450–500	2.47	6.75 ^a
200	180–212	2.47	6.75 ^a
100	90–106	2.47	6.75 ^a
50	45–53	2.47	6.75 ^a
Quartz sand			
400	355–500	2.64	4.3 ^b
100	100–140	2.64	4.3 ^b

^aPermittivity values after *von Hippel* [1954].

^bPermittivity values after *Carmichael* [1982].

two stainless steel plates 150 mm in length, 20 mm in height, 2 mm thick, and with a center spacing of 20 mm, was mounted through the end wall of the box (Figure 5). The waveguides were calibrated for effective length using deionised water in the same manner as in the work of *Heimovaara* [1993]. The geometry of parallel plates was chosen in preference to rods to give a more uniform energy distribution within the sample [*Robinson and Friedman*, 2000]. Ten waveforms were collected using the TDR device and averaged to measure the effective permittivity of the mixture.

3.3. Experimental Procedure

3.3.1. Experiment 1: Binary mixtures of 50 and 500 μm glass beads. Measurements were made using two sets of glass beads, each having a narrow size range, large (450–500 μm) and small (45–53 μm). Mixtures of the two size fractions were made according to the mass of the beads. Since the measured particle densities of the large and small beads were found to be the same (Table 1), the mass and volumetric fractions were the same. Beginning with monosize large beads, mixtures were made with 0.15 small, 0.33, 0.50, 0.66, and 0.8 through to monosize small beads. To ensure an even distribution of large and small beads in each mixture, the dry beads were sprayed with 10 g of deionized water and mixed thoroughly in a container.

Deionized water from a weighed 1 L beaker was poured into the sample container, initially covering a depth of 10 mm. The beads were carefully spooned into the water, the level of which was increased as more beads were added; careful stirring ensured even packing of the material. Excess water was removed from the top of the mixture using a syringe and placed back in the beaker of water for the mass balance. Tight packing was achieved by banging and agitating the sample container.

The weight of the sample container was recorded, and the volume was determined by pouring water into the container, on top of the mixture which was protected by a thin film, then reweighed once full with water. The water-filled porosity and dry bulk density were then calculated. This procedure was repeated in order to obtain the data sets. The temperature of the laboratory was controlled at $25^\circ\text{C} \pm 1^\circ\text{C}$, and the sample temperature was monitored.

3.3.2. Experiment 2: Quartic mixtures of 50, 100, 200, and 500 μm glass beads. The procedure laid down for experiment 1 was repeated using four size fractions of glass beads. Three mixtures were used and had mass fractions of 0.1, 0.2, 0.3, 0.4; 0.4, 0.3, 0.2, 0.1; and 0.25, 0.25, 0.25, 0.25 for the (45–53 μm), (90–106 μm), (180–212 μm), and (450–500 μm) beads, respectively.

3.3.3. Experiment 3: Binary mixtures of quartz sand. The procedure laid down for experiment 1 was repeated using quartz sand. The size fractions consisted of a coarse fraction ranging between 355 and 500 μm and a fine fraction ranging between 100 and 140 μm . In addition to monosize grains a mixture of 0.33 small (100–140 μm) particles in large (355–500 μm) particles was used.

4. Experimental Results and Discussion

The effect of particle size distribution on the effective permittivity is expected to be relatively small, for example, a 4% reduction for a binary packing with 40% porosity (Figure 2a). The challenge in this work was to measure this small effect and to experimentally demonstrate the justification of the mixing approach presented in (4a), (4b), and (4c).

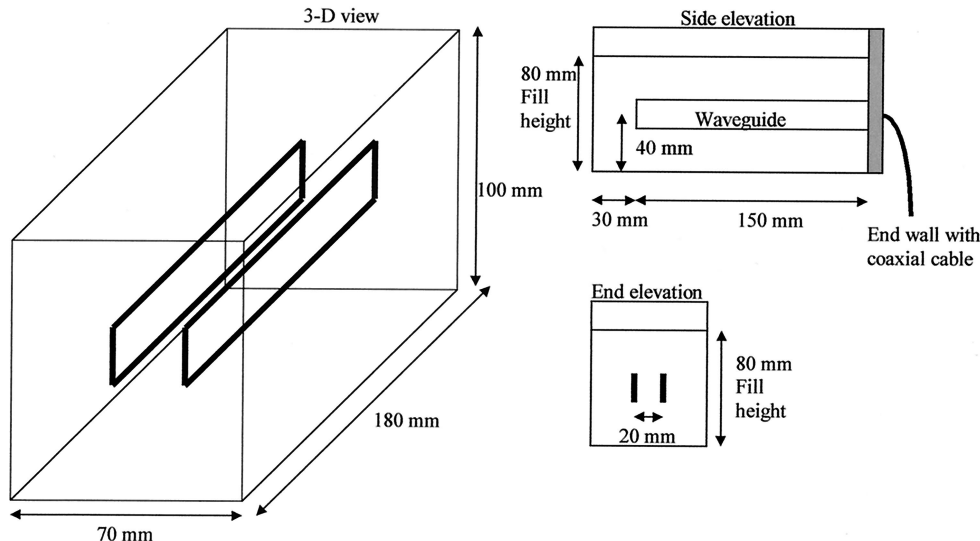


Figure 5. Schematic diagram of the cell construction showing the parallel plates contained within the measuring container constructed from plexiglass.

4.1. Results Obtained Using Glass Spheres

4.1.1. Experiment 1: Binary mixtures of 50 and 500 μm glass beads. The initial effect of mixing two particle sizes is to reduce the porosity of the mixture relative to monosize. The results demonstrating the change in porosity of a mixture with varying fractions of small spheres are shown in Figure 6. Two models are presented to describe the change of porosity with volume of fines in coarse material. The ideal packing model [Koltermann and Gorelick, 1995; Chan and Knight, 1999] splits packing into two stages; the first is when the total volume of small beads f_{small} (volume of solid plus its porosity) is less than the porosity of the large grains ϕ_{large} .

$$\phi_{\text{mix}} = \phi_{\text{large}} - f_{\text{small}}(1 - \phi_{\text{small}}) \quad f_{\text{small}} < \phi_{\text{large}}, \quad (5a)$$

where ϕ_{small} is the porosity of the small beads. The minimum porosity occurs at $f_{\text{small}} = \phi_{\text{large}}$, and its value is

$$\phi_{\text{min}} = \phi_{\text{large}}\phi_{\text{small}}. \quad (5b)$$

When f_{small} exceeds ϕ_{large} , the porosity is determined by the volume fraction of the small beads:

$$\phi_{\text{mix}} = f_{\text{small}}\phi_{\text{small}} \quad f_{\text{small}} > \phi_{\text{large}}. \quad (5c)$$

This model greatly underestimates the practical, achievable porosity, especially in the midrange. However, a semiempirical fractional packing model [Koltermann and Gorelick, 1995] with an empirical constant, $y_{\text{min}} = 0.8$, gives a reasonable fit to the data. Like the ideal packing model, it is in two parts; the first describes porosity when the total volume fraction of small spheres f_{small} is less than the porosity of the large spheres:

$$\phi_{\text{mix}} = \phi_{\text{large}} - f_{\text{small}}(y - \phi_{\text{small}}) \quad f_{\text{small}} < \phi_{\text{small}}, \quad (6a)$$

where y is an empirical coefficient reflecting the relative proportions of small and large beads. The value of y varies linearly according to

$$y = f_{\text{small}}\left(\frac{y_{\text{min}} - 1}{\phi_{\text{large}}}\right) + 1 \quad f_{\text{small}} < \phi_{\text{large}}; \quad (6b)$$

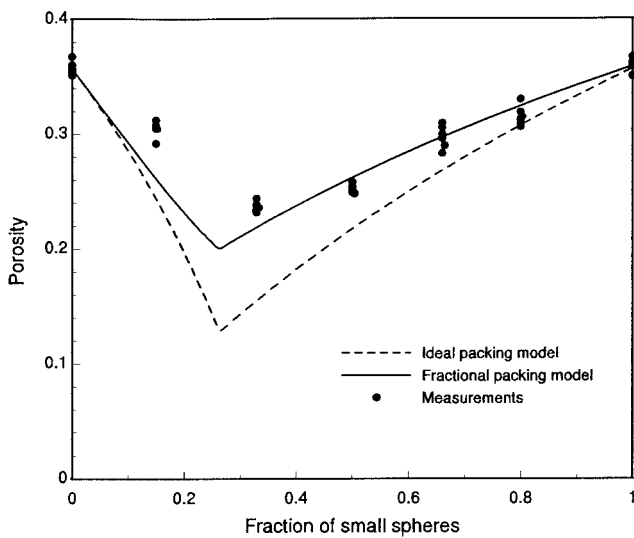


Figure 6. A comparison of the porosity of the collected data with predictions made using the ideal packing model (equation (5)) and the fractional packing model (equation (6)) with a packing coefficient of $y = 0.8$.

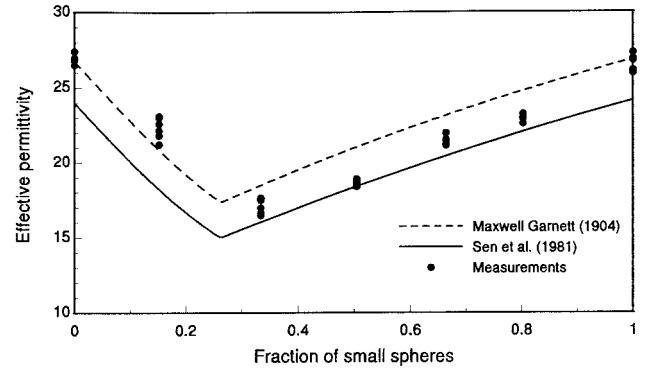


Figure 7. The effective permittivities of seven mixtures of glass beads demonstrating how they relate to the *Maxwell-Garnett* [1904] (equation (2)) and *Sen et al.* [1981] (equation (3)) models.

y_{min} in our case is expected to be 0.8 for a diameter ratio of 10 [Koltermann and Gorelick, 1995]. The minimum porosity again occurs at $f_{\text{small}} = \phi_{\text{large}}$, and its value is

$$\phi_{\text{min}} = \phi_{\text{large}}(1 - y_{\text{min}}) + \phi_{\text{large}}\phi_{\text{small}} \quad f_{\text{small}} = \phi_{\text{large}}. \quad (6c)$$

The second part is for a total volumetric fraction of small beads greater than the porosity of the large beads:

$$\phi_{\text{mix}} = \phi_{\text{large}}(1 - y) + f_{\text{small}}\phi_{\text{small}} \quad f_{\text{small}} > \phi_{\text{large}}. \quad (6d)$$

The value of y now varies linearly from y_{min} according to

$$y = (f_{\text{small}} - 1)\left(\frac{1 - y_{\text{min}}}{1 - \phi_{\text{large}}}\right) + 1 \quad f_{\text{small}} > \phi_{\text{large}}. \quad (6e)$$

This modeling approach gives a good fit to the data, an exception being for the 0.15 data, which sit above the line. This was due to some of the small beads flowing through the pores in the large beads creating a somewhat uneven distribution of the small particles in large particles on a macroscale.

The effective permittivities of the seven sets of glass bead mixtures are presented in Figure 7. The porosity, modeled by fractional packing (equations (6a)–(6e)), was used in the models describing the effective permittivity. The lines represent the predicted permittivity according to the *Maxwell-Garnett* [1904] model (dashed line) and the *Sen et al.* [1981] self-similar model (solid line) forming the expected upper and lower bounds for a solid with a permittivity of 6.75 immersed in water with a permittivity of 78.5. The higher actual porosity of the 0.15 volumetric fraction of small beads compared to that expected according to the fractional packing model is reflected here in measured permittivities slightly higher than those predicted using the packing model.

It should be noted that the binary system of 50 μm and 500 μm glass spheres referred to in the present study is quite different from the sand-clay mixtures discussed by *Knoll and Knight* [1994] and *Knoll et al.* [1995], since the clay particles in those studies were nonspherical and usually smaller than the sand grains by a factor much greater than 10. The clays may have formed into aggregated (floculated) states, rather than having been single particles. There is also likely to have been an effect caused by bound water on these clay particles, which can seriously reduce the permittivity of the water in contact with the clay plates. Therefore one should not directly infer

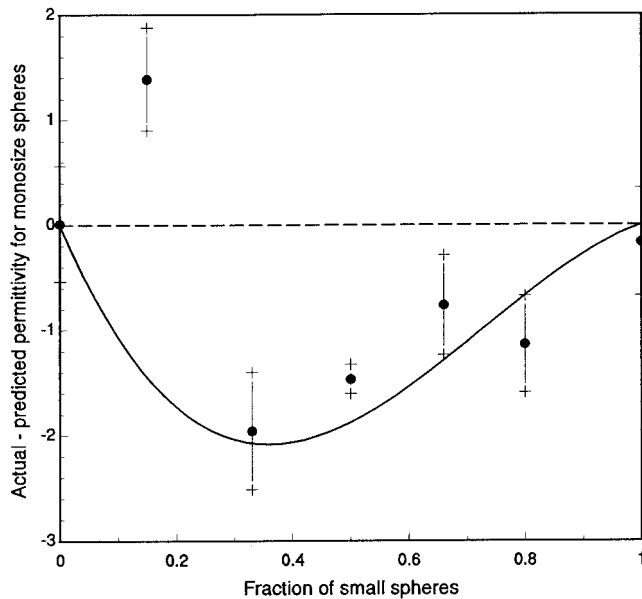


Figure 8. Measured permittivity minus the permittivity predicted using the Maxwell-Garnett model (equation (2)). Note the similarity in shape of the fitted polynomial (solid line) to Figure 2a.

from the results of the present study to mixtures of sand, silt, and clay particles constituting real soils.

Figure 8 subtracts the predicted permittivity using the Maxwell-Garnett model for a packing of monosize spheres of the same porosity from the measured permittivities. The reduced permittivity from that of monosize can clearly be seen as the particle size distribution changes other than for a small fraction of 0.15 where the value is positive because of the flow of the fine through the coarse as mentioned. The permittivity of the mixture is reduced by ~ 2 , going from monosize to one third small particles mixed in large particles. This is very similar to the pattern derived from theory and presented in Figure 2a for fixed porosities.

Figure 9 presents the measured effective permittivities of the mixtures of large and small beads against the actual porosities of the mixtures. The Maxwell-Garnett and Sen et al. models are plotted defining the expected upper and lower bounds. The Maxwell-Garnett model is plotted down to a minimal porosity of 0.26 representing the porosity of a face-centered cubic packing of monosize spheres. The data for both small and large monosize spheres packed to different porosities can clearly be seen to follow the line predicted by the Maxwell-Garnett model, the unexpected close fit suggests that the permittivity value of 6.75 used for the solid is perhaps low and is being investigated. A value of 0.35 was found to be the minimum achievable porosity using monosize beads. As the mixing of small beads into large occurs, so the data can be seen to diverge from the Maxwell-Garnett prediction toward that of Sen et al. and then converge back to the Maxwell-Garnett prediction as the mixing progresses to monosize small beads. The prediction of the two-step mixing model (equations (4a), (4b), and (4c)), represented by a cross for each of the data groups and connected with cubic splines, follows the pattern of the data, lying slightly above the measured values, which is very acceptable agreement considering the inherent experimental difficulties.

4.1.2. Experiment 2: Quartic mixtures with 50, 100, 200, and 500 μm glass beads. The results using mixtures of four sizes of glass beads with the same width of particle size distribution as in experiment 1 (50–500 μm) are presented in Figure 10. These mixtures present a more continuous particle size distribution, compared to the bimodal one of experiment 1. The three mixtures represent uniform (circles), increasing (solid triangles), and decreasing (open triangles) particle size distributions. Again, the Maxwell-Garnett and Sen et al. models provide an upper and lower bound. The data for the monosize spheres are the same as presented in Figure 9. All three mixtures again show the reduction in the permittivity compared to monosize packing. Again, crosses are used to represent the prediction of the four-step mixing (equation (4c)), joined together with cubic splines. The results using the limited mixing approach are in remarkably good agreement with the data.

4.2. Results Obtained Using Quartz Sand

Figure 11 presents results collected using acid-washed quartz sand grains. The Maxwell-Garnett and Sen et al. models present the expected upper and lower bounds for a solid with a permittivity of 4.3. The effective permittivity values calculated by the two-step mixing for a binary mixture of spheres are presented in Figure 11; below these calculated values are effective permittivity values with 1.6 subtracted to demonstrate agreement with the measured permittivity values for the packings. We believe that this initial reduction of 1.6 from the permittivity is due to the reduced sphericity of the sand grains and is something we discuss briefly but hope to explore further in future work.

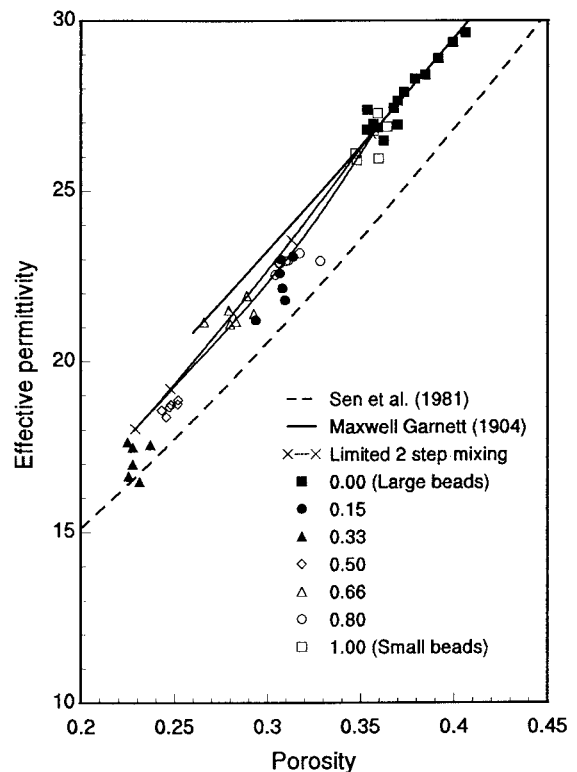


Figure 9. Measurements of the effective permittivity of binary mixtures of glass beads at saturation and the predictions by the Maxwell-Garnett and Sen et al. models and the presented two-step mixing method.

It is clear that the data of the monosize grains do not fall on the Maxwell-Garnett prediction assuming spherical inclusions with an ϵ_s of 4.3. It is probably the less regular and spherical shape of the sand grains that reduces the effective permittivity of both the monosize packing and the mixtures. Knowing the Maxwell-Garnett predictions for glass spheres appear accurate, an effective aspect ratio can be determined for an isotropic packing of oblate ellipsoids of revolution [Sihvola and Kong, 1988; Jones and Friedman, 2000]. An aspect ratio of 4 (4:4:1, disk-shaped particles) was determined to give an upper bound; this is not to say that the particles are ellipsoids of this shape but that the effect that they have on the shape of the water bodies is equivalent to oblate ellipsoids with this aspect ratio. This suggests that factors such as grain angularity and surface roughness are contributing factors to lowering the permittivity and should be included in models such as that of Friedman [1998].

5. Conclusions

Measurements carried out with mixtures of glass beads and sand grains of different size demonstrated that particle size distribution has a small but measurable effect on the effective permittivity of saturated, unconsolidated porous media. A limited-mixing approach based on the Maxwell-Garnett model was found to adequately describe the effective permittivity of mixtures of different sizes of glass beads. The modeling demonstrates that the permittivity of a bimodal mixture of glass spheres may be reduced by about 4% compared to the equivalent monosize packing. For most practical measurements this effect can be neglected; however, in some highly sorted mate-

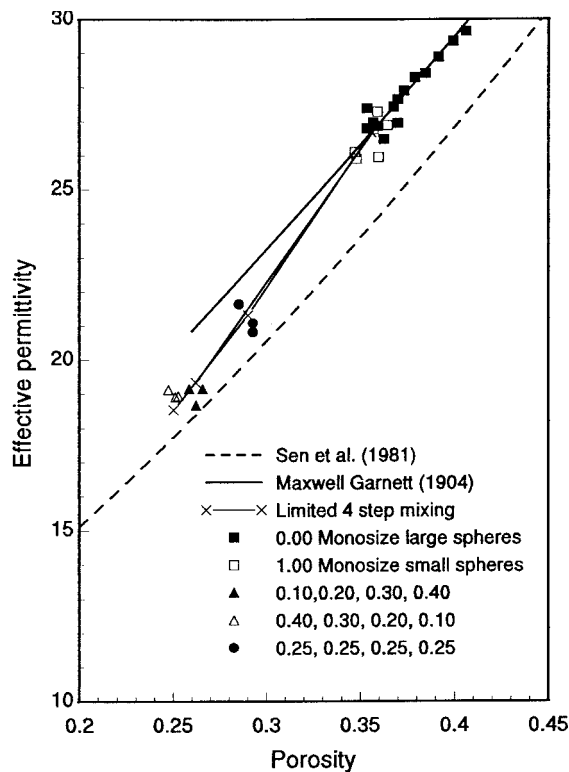


Figure 10. Measurements of the effective permittivity of quartic mixtures of glass beads at saturation and the predictions by the Maxwell-Garnett and Sen et al. models and the presented four-step mixing method.

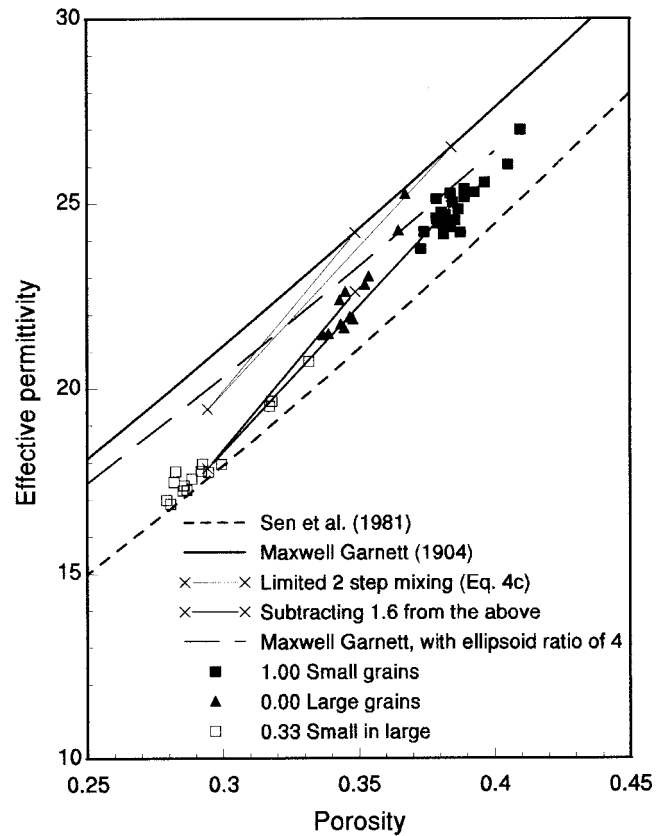


Figure 11. Measurements of the effective permittivity of binary mixtures of quartz sand at saturation and the predictions by the Maxwell-Garnett and Sen et al. models and the presented two-step mixing method.

rials it might be considered as a source of potential error in estimating porosity from permittivity measurements. The theory provided and experimental results give a good explanation as to why effective permittivity measurements for different samples of the same material but of different degree of sorting may differ slightly at saturation, above and beyond the effect of porosity.

Acknowledgments. The authors wish to acknowledge the funding provided for this project from the BARD (Project IS-2839-97), The United States-Israel Binational Agricultural Research and Development Fund. Contribution 611/00 from the Agricultural Research Organization, The Volcani Center, Bet Dagan, Israel. We are also grateful to Scott Jones for his assistance in the initial stages of this study and for the comments provided in review by J. D. Cooper and the other anonymous reviewers.

References

- Archie, G. E., The electrical resistivity log as an aid in determining some reservoir characteristics, *Trans. Am. Inst. Min. Metall. Pet. Eng.*, 146, 54–62, 1942.
- Carmichael, R. S., *Handbook of Physical Properties of Rocks*, CRC Press, Boca Raton, Fla., 1982.
- Chan, C. Y., and R. Knight, Determining water content and saturation from dielectric measurements in layered materials, *Water Resour. Res.*, 35(1), 85–93, 1999.
- Chew, W. C., and P. N. Sen, Dielectric enhancement due to electrochemical double layer: Thin double layer approximation, *J. Chem. Phys.*, 77(9), 4683–4693, 1982.
- Chiew, Y. C., and E. D. Glandt, Effective conductivity of dispersions:

- The effect of resistance at the particle surfaces, *Chem. Eng. Sci.*, 42(11), 2677–2685, 1987.
- Friedman, S. P., A saturation degree-dependent composite spheres model for describing the effective dielectric constant of unsaturated porous media, *Water Resour. Res.*, 34(11), 2949–2961, 1998.
- Guyon, E., L. Oger, and T. J. Plona, Transport properties in sintered porous media composed of two particle sizes, *J. Phys D Appl. Phys.*, 20, 1637–1644, 1987.
- Heimovaara, T. J., Time domain reflectometry in soil science: Theoretical backgrounds, measurements and models, Ph.D. thesis, Univ. van Amsterdam, Amsterdam, Netherlands, 1993.
- Jones, S. B., and S. P. Friedman, Particle shape effects on the effective permittivity of anisotropic or isotropic media consisting of aligned or randomly oriented ellipsoidal particles, *Water Resour. Res.*, 36(10), 2821–2833, 2000.
- Knoll, M. D., and R. Knight, Relationships between dielectric and hydrogeologic properties of sand clay mixtures, in *Proceedings of the International Conference on Ground Penetrating Radar*, pp. 45–61, Waterloo Cent. for Groundwater Res., Univ. of Waterloo, Waterloo, Ont., Canada, 1994.
- Knoll, M. D., R. Knight, and E. Brown, Can accurate estimates of permeability be obtained from measurements of dielectric properties?, paper presented at Symposium on the Application of Geophysics to Environmental and Engineering Problems, Environ. and Eng. Geophys. Soc., Orlando, Fla., April 23–26, 1995.
- Koltermann, C. E., and S. M. Gorelick, Fractional packing model for hydraulic conductivity derived from sediment mixtures, *Water Resour. Res.*, 31(12), 3283–3297, 1995.
- Kraszewski, A. W., and S. O. Nelson, Moisture content determination in single kernels and seeds with microwave resonant sensors, in *Microwave Aquametry Electromagnetic Wave Interaction with Water-Containing Materials*, edited by A. W. Kraszewski, pp. 177–203, IEEE Press, Piscataway, N. J., 1996.
- Lange, N. A. (Ed.), *Langes Handbook of Chemistry*, 10th ed., McGraw-Hill, New York, 1966.
- Lemaitre, J., J. P. Troadec, D. Bideau, A. Gervois, and E. Bougault, The formation factor of the pore space of binary mixtures of spheres, *J. Phys. D Appl. Phys.*, 21, 1589–1592, 1988.
- Masch, F. D., and K. J. Denny, Grain size distribution and its effect on the permeability of unconsolidated sands, *Water Resour. Res.*, 2(4), 665–677, 1966.
- Maxwell-Garnett, J. C., Colours in metal glasses and in metallic films, *Philos. Trans. R. Soc. London, Ser. A*, 203, 385–420, 1904.
- Poley, J. P., J. J. Nootboom, and P. J. de Waal, Use of VHF dielectric measurement for borehole formations analysis, *Log Anal.*, 8–30, 1978.
- Rayleigh, Lord (J. W. Strutt), On the influence of obstacles arranged in rectangular order upon the properties of the medium, *Philos. Mag.*, 34, 481–502, 1892.
- Robinson, D. A., and S. P. Friedman, Parallel plates compared to conventional rods as TDR waveguides for sensing soil moisture, *Subsurf. Sens. Technol. Appl.*, in press, 2000.
- Sen, P. N., C. Scala, and M. H. Cohen, A self-similar model for sedimentary rocks with application to the dielectric constant of fused glass beads, *Geophysics*, 46(5), 781–795, 1981.
- Sihvola, A., Dielectric mixture theories in permittivity prediction: Effect of water on macroscopic parameters, in *Microwave Aquametry Electromagnetic Wave Interaction With Water-Containing Materials*, edited by A. W. Kraszewski, pp. 111–121, IEEE Press, Piscataway, N. J., 1996.
- Sihvola, A., A review of dielectric mixing models, *Rep. 248*, Dep. of Electr. and Commun. Eng., Helsinki Univ. of Technol., Espoo, Finland, 1997.
- Sihvola, A., and J. A. Kong, Effective permittivity of dielectric mixtures, *IEEE Trans. Geosci. Remote Sens.*, 26(4), 420–429, 1988.
- Topp, G. C., J. L. Davis, and A. P. Annan, Electromagnetic determination of soil water content: Measurements in coaxial transmission lines, *Water Resour. Res.*, 16(3), 574–582, 1980.
- Tyc, S., M. S. Lawrence, P. N. Sen, and P. Wong, Geometrical models for the high-frequency dielectric properties of brine saturated sandstones, *J. Appl. Phys.*, 64(5), 2575–2581, 1988.
- von Hippel, A. R. (Ed.), *Dielectrics Materials and Applications*, MIT Press, Cambridge, Mass., 1954.

S. P. Friedman and D. A. Robinson, Department of Environmental Physics and Irrigation, The Institute of Soil, Water and Environmental Sciences, The Volcani Center, Bet Dagan 50-250, Israel. (vwdrobin@agri.gov.il)

(Received November 1, 1999; revised June 2, 2000; accepted July 25, 2000.)